AGU PUBLICATIONS

JGR

Journal of Geophysical Research: Space Physics

RESEARCH ARTICLE
10.1002/2015JA022013

Photochemistry of forbidden oxygen lines in the inner coma of 67P/Churyumov-Gerasimenko

G. Cessateur[1], J. De Keyser[1,2], R. Maggiolo[1], A. Gibbons[1,3], G. Gronoff[4,5], H. Gunell[1], F. Dhooghe[1], J. Loreau[3], N. Vaeck[3], K. Altwegg[6,7], A. Bieler[6,8], C. Briois[9], U. Calmonte[6], M. R. Combi[8], B. Fiethe[10], S. A. Fuselier[11,12], T. I. Gombosi[8], M. Hässig[6,11], L. Le Roy[6], E. Neefs[13], M. Rubin[6], and T. Sémon[6]

[1]Space Physics Division, Royal Belgian Institute for Space Aeronomy, Brussels, Belgium, [2]Center for Plasma Astrophysics, Katholieke Universiteit Leuven, Heverlee, Belgium, [3]Service de Chimie Quantique et Photophysique, Université Libre de Bruxelles, Brussels, Belgium, [4]Science Directorate, Chemistry and Dynamics Branch, NASA Langley Research Center, Hampton, Virginia, USA, [5]SSAI, Hampton, Virginia, USA, [6]Physikalisches Institut, University of Bern, Bern, Switzerland, [7]Center for Space and Habitability, University of Bern, Bern, Switzerland, [8]Department of Climate and Space Sciences and Engineering, University of Michigan, Ann Arbor, Michigan, USA, [9]Laboratoire de Physique et Chimie de l'Environnement et de l'Espace, UMR 7328 CNRS, Université dOrléans, Orléans, France, [10]Institute of Computer and Network Engineering (IDA), TU Braunschweig, Braunschweig, Germany, [11]Space Science Division, Southwest Research Institute, San Antonio, Texas, USA, [12]Department of Physics and Astronomy, University of Texas at San Antonio, San Antonio, Texas, USA, [13]Engineering Division, Royal Belgian Institute for Space Aeronomy, Brussels, Belgium

Key Points:
- The presence of O_2 within 67P's atmosphere increases significantly the red line emission
- Estimations of CO_2 abundances based on the G/R ratio should be revised due to the O_2 presence
- Space weather phenomena such as solar flares have an impact on the comet photochemistry

Correspondence to:
G. Cessateur,
gael.cessateur@aeronomie.be

Citation:
Cessateur, G., et al. (2016), Photochemistry of forbidden oxygen lines in the inner coma of 67P/Churyumov-Gerasimenko, *J. Geophys. Res. Space Physics*, *121*, 804–816, doi:10.1002/2015JA022013.

Received 7 OCT 2015
Accepted 24 DEC 2015
Accepted article online 14 JAN 2016
Published online 28 JAN 2016
Corrected 9 MAR 2016
Corrected 29 MAR 2016

This article was corrected on 9 MAR 2016 and 29 MAR 2016. See the end of the full text for details.

Abstract Observations of the green and red-doublet emission lines have previously been realized for several comets. We present here a chemistry-emission coupled model to study the production and loss mechanisms of the O(^{1}S) and O(^{1}D) states, which are responsible for the emission lines of interest for comet 67P/Churyumov-Gerasimenko. The recent discovery of O_2 in significant abundance relative to water 3.80 ± 0.85% within the coma of 67P has been taken into consideration for the first time in such models. We evaluate the effect of the presence of O_2 on the green to red-doublet emission intensity ratio, which is traditionally used to assess the CO_2 abundance within cometary atmospheres. Model simulations, solving the continuity equation with transport, show that not taking O_2 into account leads to an underestimation of the CO_2 abundance within 67P, with a relative error of about 25%. This strongly suggests that the green to red-doublet emission intensity ratio alone is not a proper tool for determining the CO_2 abundance, as previously suggested. Indeed, there is no compelling reason why O_2 would not be a common cometary volatile, making revision of earlier assessments regarding the CO_2 abundance in cometary atmospheres necessary. The large uncertainties of the CO_2 photodissociation cross section imply that more studies are required in order to better constrain the O(^{1}S) and O(^{1}D) production through this mechanism. Space weather phenomena, such as powerful solar flares, could be used as tools for doing so, providing additional information on a good estimation of the O_2 abundance within cometary atmospheres.

1. Introduction

Comets are physicochemical witnesses of the conditions of the early solar system, and their study can bring us valuable information concerning solar system formation theories. Comet researchers usually have to resort to remote observations. Numerous studies have been devoted to the direct observation of atomic oxygen lines [*Morgenthaler et al.*, 2007; *Cochran*, 2008; *McKay et al.*, 2015]. Photodissociation of H_2O, CO_2, and CO results in the release of an oxygen atom in an excited state, either O(^{1}D) or O(^{1}S). The emission lines of interest are the radiative transition from O(^{1}D) to O(^{3}P), which is responsible for the formation of the double red line emission at 630 and 636.4 nm and the deactivation of the O(^{1}S) state leading to the green line emission at 557.7 nm. In that regard, the CO_2 abundance relative to the H_2O abundance has been previously inferred from remote sensing data by taking the ratio between the intensities of the excited atomic oxygen green and red-doublet emission lines in comets (hereafter G/R ratio) [*McKay et al.*, 2012, 2013; *Decock et al.*, 2013, 2015]. Up until now, the photodissociation of other major volatiles such as water, carbon dioxide, the hydroxyl radical, and carbon monoxide have been considered as the main processes for producing O(^{1}S) and O(^{1}D) atoms [see, e.g., *Bhardwaj and Raghuram*, 2012, and references therein].

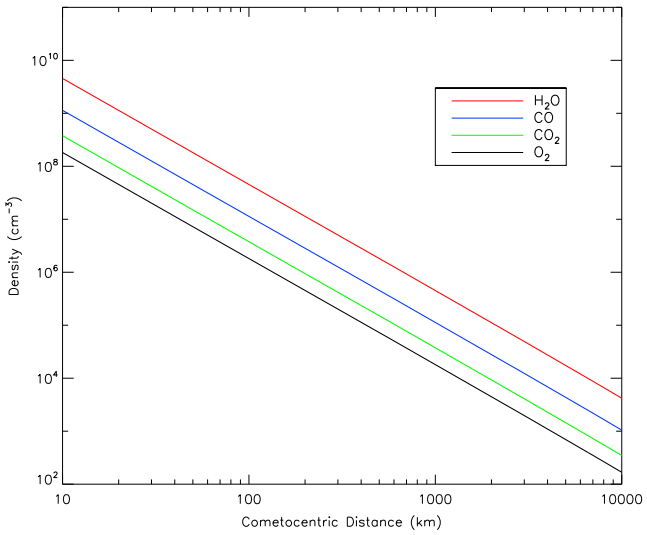

Figure 1. Number densities considered in the model based on the ROSINA/DFMS data and on Haser's formula, for water (red), CO (blue), O_2 (black), and CO_2 (green) using a water production rate of 4×10^{27} s^{-1} and an outgassing speed of 700 m s^{-1} at 1.35 AU heliocentric distance.

The Double Focusing Mass Spectrometer (DFMS), part of the Rosetta Orbiter Sensor for Ion and Neutral Analysis (ROSINA), on board the Rosetta spacecraft, is a high-resolution mass spectrometer allowing the precise analysis of the cometary exosphere (or coma) of comet 67P/Churyumov-Gerasimenko (hereafter 67P) [*Balsiger et al.*, 2007]. DFMS has already delivered several important results, for instance, the D/H ratio in water in 67P [*Altwegg et al.*, 2015] and the discovery of N_2 [*Rubin et al.*, 2015] and O_2 [*Bieler et al.*, 2015]. Even though the Rosetta mission is a unique opportunity to study one comet up close, the results it delivers are likely to be applicable to other comets as well. For instance, the detection of O_2 has been possible in 67P thanks to in situ mass spectrometry with the very high mass resolution and sensitivity of DFMS. Since there is no compelling reason to consider 67P unique, this would suggest that molecular oxygen is also present in other cometary atmospheres. This molecule has never been considered in coupled chemistry-emission models determining the G/R ratio. However, the photodissociation of O_2 is also an important source of $O(^1S)$ and $O(^1D)$, and should therefore be taken into account. The goal of this paper is first to assess the impact of previously undetected molecules such as O_2 on the production of excited oxygen states $O(^1S)$ and $O(^1D)$, and on the $O(^1S)$ to $O(^1D)$ ratio as a function of the cometocentric distance. We furthermore discuss the implication of the presence of O_2 on previous cometary models and observations. Finally, we explore the impact of the CO_2 cross-section uncertainties on the G/R ratio as well as the impact of the solar UV flux within a planetary space weather context.

2. Chemistry-Emission Coupled Model

The purpose of this section is to describe the chemistry-emission coupled model for 67P. We use the spherically symmetric expansion model of *Haser* [1957] to estimate the number densities $n_i(r)$ of the ith parent species at a cometocentric distance r from the nucleus. The water production rate from the surface of 67P near perihelion has been estimated at 4×10^{27} s^{-1} for July 2015, while the velocity of the escaping volatiles has been measured to be 700 m s^{-1} using the data of the Comet Pressure Sensor, part of the ROSINA experiment. We consider the primary volatile elements detected by the ROSINA/DFMS spectrometer, H_2O, CO_2, CO, and O_2.

The average CO and CO_2 abundances relative to water have been estimated at 25% and 8.3% for the month of July 2015. Those abundances are in bulk agreement with the values presented by *Hässig et al.* [2015] and *Le Roy et al.* [2015]. The detection of O_2, as discussed by *Bieler et al.* [2015], will have an impact on the production rate of the atomic states $O(^1D)$ and $O(^1S)$. The ROSINA/DFMS instrument on board Rosetta has indeed detected the presence of O_2 in high quantity, with an abundance relative to water of 3.80 $\pm$ 0.85%, which puts this volatile in an abundance range comparable to that of CO_2. An average O_2 abundance of 4%, as measured in July 2015, will be considered in the following. The resulting neutral atmosphere is displayed in Figure 1.

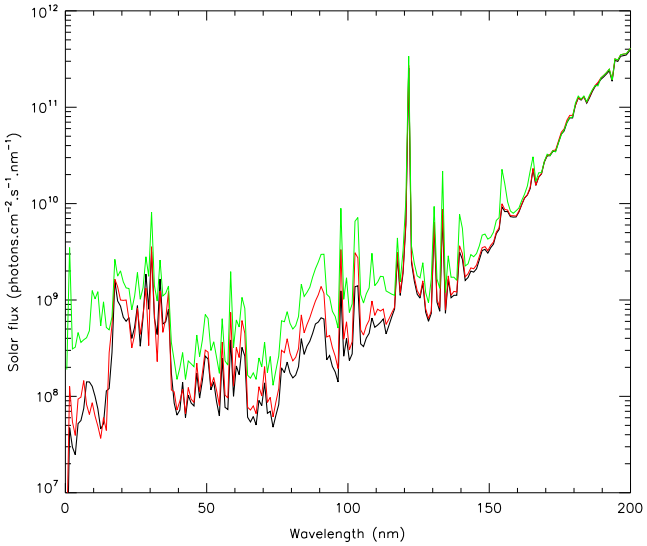

Figure 2. Solar UV fluxes for a heliocentric distance of 1.35 AU heliocentric distance for July 2015 (black curve), for high solar activity condition with $F_{10.7} = 195$ (red curve), and for the X17 flare occurring on 28 October 2003 (green curve).

2.1. Production Reactions

The dominant source of the production of O(^{1}D) and O(^{1}S) in the inner coma ($\lesssim 10^4$ km) is the photodissociation of the major oxygen-bearing volatile components [see, e.g., *Decock et al.*, 2015]. A simple model for evaluating the green and red-doublet line emissions within 67P's atmosphere as a function of the nucleocentric distance is presented here. We consider only the impact of the solar UV flux on the production of the three forbidden oxygen lines of interest. The photoelectron impact dissociative excitation of volatile components was shown to make only a minor contribution ($\lesssim$1%) in the inner coma [see, e.g., *Bhardwaj and Raghuram*, 2012]. The ion recombination reactions and photodissociation of hydroxyl also have a minor contribution to the production of O(^{1}D) and O(^{1}S) in the inner coma. We consider a heliocentric distance of about 1.35 AU for 67P, corresponding to its position in the solar system in July 2015 not far from perihelion. A composite solar spectrum from 1 to 300 nm with 1 nm bin resolution is used, scaled to a heliocentric distance of 1.35 AU using an inverse distance-square law, based on the observations of three instruments in Earth orbit. Data in the 1–27 nm range come from the *XUV Photometer System* [*Woods et al.*, 2008] on board the *SOLar Radiation and Climate Experiment* (SORCE) [*Rottman*, 2005]. The 27–115 nm range data are taken from the *Solar Extreme Ultraviolet Experiment* (SEE) on board TIMED [*Woods et al.*, 2005]. Finally, the spectral range 115–300 nm comes from the *SOLar Stellar Irradiance Comparison Experiment* [*McClintock et al.*, 2005], also on board the SORCE spacecraft. The composite solar UV spectrum is displayed in Figure 2 (black curve), and the corresponding level of solar activity in terms of the $F_{10.7}$ index is about 104 for July 2015.

In order to take account for the attenuation of solar radiation by the cometary atmosphere at wavelength λ and altitude z, a Beer-Lambert law is considered:

$$F(\lambda, z) = F_{\infty}(\lambda) e^{-\tau_{\mathrm{tot}}(z,\lambda)}, \tag{1}$$

where $F_{\infty}(\lambda)$ is the solar UV flux at the top of the cometary atmosphere, taken at 10^4 km from the nucleus. We use a grid with adaptive mesh size ranging from 1 km close to the surface to 10 km far from the comet. The solar UV flux at each altitude z from the nucleus is computed taking into account the wavelength-dependent total photoabsorption cross section for the different neutral species, used for computing the optical depth $\tau(z)_{\mathrm{tot}}$. The different total cross sections relative to water, carbon monoxide, carbon dioxide, and molecular oxygen are taken from the PHIDRATES database (see http://phidrates.space.swri.edu/) which is based on the work of *Huebner and Mukherjee* [2015]. The solar UV flux is mostly absorbed in the spectral range between 60 and 100 nm with an absorption average of about 12.5% between the top of the atmosphere and at 10 km above the comet, with a maximum at 90 nm with 17% of absorbed flux. Above 100 nm, the solar UV flux is mostly absorbed until 130 nm mainly because of the presence of water and O_2 with an average absorption of about 5%.

Table 1. Major Production Reactions of $O(^1D)$ and $O(^1S)$, and Associated Reaction Rate Coefficients (in s^{-1})[a]

Reaction	Rate Coefficients
$H_2O + h\nu \longrightarrow O(^1D) + H_2$	4.91×10^{-7} (−3%)
$CO_2 + h\nu \longrightarrow O(^1D) + CO$	5.52×10^{-7} (−7.3%)
$CO + h\nu \longrightarrow O(^1D) + C$	2.28×10^{-8} (−11.8%)
$O_2 + h\nu \longrightarrow O(^1D) + O$	1.46×10^{-6} (−1.21%)
$H_2O + h\nu \longrightarrow O(^1S) + H_2$	2.55×10^{-8} (−2.7%)
$CO_2 + h\nu \longrightarrow O(^1S) + CO$	2.93×10^{-7} (−8.24%)
$CO + h\nu \longrightarrow O(^1S) + C$	1.78×10^{-8} (−11.8%)
$O_2 + h\nu \longrightarrow O(^1S) + O$	4.5×10^{-9} (−8.92%)

[a]The photolysis rate coefficients are given at the top of the atmosphere and the differences between the top of the atmosphere and at 10 km altitude are indicated in parentheses.

The production rates coefficients for an atomic state *a*, i.e., $O(^1D)$ or $O(^1S)$ from the photodissociation of the considered species *i*, i.e., water, carbon dioxide, molecular oxygen, and carbon monoxide, are computed using the following equation:

$$k^a(z) = \int_\lambda \sigma_a^i(\lambda) F(\lambda, z) \mathrm{d}\lambda \tag{2}$$

where $\sigma_a^i(\lambda)$, are the partial cross sections leading to the photoproduction of the atomic states $O(^1D)$ and $O(^1S)$, also taken from the PHIDRATES database for water, carbon dioxide, and carbon monoxide.There is still, however, an ongoing discussion regarding the $O(^1S)$ production through the photodissociation of water. For the sake of comparison, we follow here the approach used by *Bhardwaj and Raghuram* [2012], assuming a 0.5% yield at 121.6 nm. Regarding the production of $O(^1S)$ from CO_2, the considered partial cross section is obtained by multiplying the total cross section of CO_2 by the yield recommended by *Huestis et al.* [2010]. Regarding the production of $O(^1S)$ from the photodissociation of CO, we also follow the approach from *Bhardwaj and Raghuram* [2012] since no partial cross-section data are available in the PHIDRATES database. The computed production rate coefficients at the top of the cometary atmosphere are summarized in Table 1, for a heliocentric distance of 1.35 AU. With the number densities prevailing in 67P's atmosphere, the solar flux is attenuated in such a way that there is a difference of about 2.7–3% between the production rate coefficients from water at the top of the atmosphere compared to 10 km altitude. The solar UV flux is more absorbed for wavelengths between 70 and 90 nm, leading to a more pronounced decrease of the production rates from CO_2 and CO of about 8% and 12%, respectively.

The presence of O_2 is taken into account here for the first time in such modeling. The photodissociation of O_2 follows three principal channels for the wavelengths of interest. Above 177 nm, only the $O(^3P)$ ground state is produced. For the wavelength range from 115 nm to 177 nm, the photoproducts are $O(^1D)$ and $O(^3P)$ and the production yield is taken from *Lee et al.* [1977]. Below 115 nm down to 90 nm, photodissociation results in $O(^1S)$ and $O(^3P)$, and the recommended cross section from the ATMOCIAD database is used [*Gronoff et al.*, 2011]. This set of cross section, available upon request, has been widely used within an aeronomic context for modeling the Mars airglow [*Gronoff et al.*, 2012a, 2012b], in a cometary studies context for the comet Siding Spring [*Gronoff et al.*, 2014] and more recently used for retrieving carbon dioxide and molecular nitrogen for the upper atmosphere of Mars using the Imaging Ultraviolet Spectrograph (IUVS) on board NASA's Mars Atmosphere and Volatile Evolution spacecraft [*Evans et al.*, 2015]. At a distance of 1.35 AU and for a solar flux corresponding to a solar activity of $F_{10.7} = 104$, the computed reaction rates at the top of the atmosphere are 1.46×10^{-6} s^{-1} and 4.5×10^{-9} s^{-1} for the photoproduction of $O(^1D)$ and $O(^1S)$, respectively. The attenuation of the solar UV flux in this case leads, respectively, to a 1.21% and 8.92% decrease.

The calculated $O(^1D)$ and $O(^1S)$ production rate profiles are presented in Figure 3. The major source of $O(^1D)$ in the inner coma is clearly the photodissociation of water, with a production rate of 2×10^3 cm^{-3} s^{-1} at 10 km from the nucleus. A secondary contribution comes from the photodissociation of CO_2, but represents only 10% of the total produced $O(^1D)$. The photodissociation of O_2 plays also a minor role compared to water but is as large as the contribution of CO_2 and represents 10% of the total $O(^1D)$ production. The photodissociation of CO is clearly a minor process, representing roughly 1% of the total. The radiative decay of $O(^1S)$ leads also to

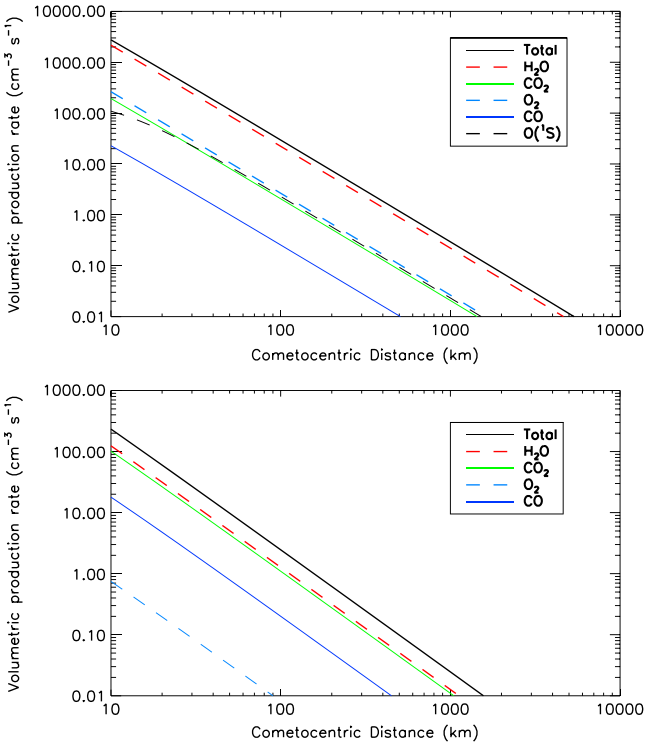

Figure 3. (top) Calculated radial profiles for the volumetric production of O(^{1}D) (black) from 10 to 10^4 km, along with its contribution from the photodissociation of water (red dashed line), of CO_2 (green), of O_2 (blue dashed line), and of CO (dark blue). The contribution to the O(^{1}D) production through radiative decay of O(^{1}S) is also displayed (dashed black line). (bottom) Same color code for the production of O(^{1}S). The radial profiles are calculated with a water production rate of 4×10^{27} s^{-1} for 25% CO, 8.3% CO_2, and 4% of O_2 abundances relative to water at 1.35 AU heliocentric distance.

the production of O(^{1}D), through reaction 9 in Table 2. As discussed in section 2.2, this is an effective process with a contribution equivalent to the photodissociation of CO_2 and O_2 producing atomic oxygen O(^{1}D).

Both the photodissociation of water and CO_2 are important O(^{1}S) sources for 67P. Indeed, the number density of CO_2 is high enough to play a major role along with water. This has already been modeled for comets with similar atmospheric compositions (see, e.g., comets C/2003 K4 (LINEAR) and 116P/Wild 4 as discussed by *Raghuram and Bhardwaj* [2014]). The total production of O(^{1}S) close to the nucleus at 10 km is about 2×10^2 cm^{-3} s^{-1}. The photodissociation of CO leading to O(^{1}S) is a secondary process with a contribution of 10%. The photodissociation of O_2 plays only a minor role, with less than 1% of the total produced O(^{1}S).

We also looked which parts of the solar UV flux influence the production of O(^{1}D) and O(^{1}S). When considering the neutral densities presented in Figure 1, the solar UV at Lyman α is responsible for 70% of the production of O(^{1}D), coming mainly from the photodissociation of water. The following spectral bands [80–100 nm], [122–140 nm], and [141–180 nm] account fairly for 18% to the production of O(^{1}D), while the spectral range [101–120 nm] contribution is 8%. Regarding the production of O(^{1}S), the solar Lyman α line accounts for 45% while the spectral band [90–115 nm] is responsible for 40%. The spectral band between 60 and 90 nm represents roughly 13% of the production.

2.2. Loss Reactions

While the production reactions are mainly photolysis processes, loss reactions of atomic oxygen O(^{1}D) and O(^{1}S) are either collisional processes or radiative decays. Collisional quenching by water is the predominant loss reaction in the inner coma, while the radiative processes are very effective far from the nucleus [see, e.g., *Bhardwaj and Raghuram*, 2012]. Table 2 summarizes the major loss reactions of the oxygen states O(^{1}D) and O(^{1}S) taken into account in the present model when considering water, carbon monoxide, molecular oxygen, and carbon dioxide. The associated rate coefficients are also summarized in Table 2, and computed for a temperature of 50 K. In the case of the volatile densities of 67P near perihelion, the oxygen state O(^{1}D) begins to be efficiently quenched by water for altitudes below 400 km with a maximal loss rate of about 1 s^{-1}

Table 2. Major Loss Reactions of $O(^1D)$ and $O(^1S)$ and Associated Rate Coefficients Computed With the Composite Solar Spectrum at 1.35 AU Heliocentric Distance and the Different Partial Cross Sections Described Within the Text

Reaction	Rate Coefficients[a]
(1) $O(^1D) + H_2O \longrightarrow OH + OH$	$k_1 = 2.2 \times 10^{-10}$
(2) $O(^1D) + CO_2 \longrightarrow O + CO_2$	$k_2 = 6.8 \times 10^{-11} e^{-117/T}$
(3) $O(^1D) + CO \longrightarrow O + CO$	$k_3 = 5.5 \times 10^{-10} e^{-625/T}$
(4) $O(^1D) \longrightarrow O(^3P) + h\nu$ (630 nm)	$A_1 = 6.478 \times 10^{-3}$
(5) $O(^1D) \longrightarrow O(^3P) + h\nu$ (634.4 nm)	$A_2 = 2.097 \times 10^{-3}$
(6) $O(^1D) + O_2 \longrightarrow O(^3P) + O_2$	$k_{11} = 3.2 \times 10^{-11}$
(7) $O(^1S) + H_2O \longrightarrow OH + OH$	$k_6 = 3 \times 10^{-10}$
(8) $O(^1S) + CO_2 \longrightarrow O + CO_2$	$k_7 = 3.1 \times 10^{-11} e^{-1330/T}$
(9) $O(^1S) + CO \longrightarrow O + CO$	$k_8 = 3.21 \times 10^{-12} e^{-1327/T}$
(10) $O(^1S) \longrightarrow O(^1D) + h\nu$ (557.7 nm)	$A_3 = 1.26$
(11) $O(^1S) \longrightarrow O(^3P) + h\nu$ (297.7 nm)	$A_4 = 0.134$
(12) $O(^1S) + O_2 \longrightarrow O(^3P) + O_2$	$k_{12} = 3.2 \times 10^{-13}$

[a]Units are in $cm^3\ s^{-1}$ for two-body reactions, A_i are in s^{-1}. k_i are from *Atkinson et al.* [2004]. Einstein transition probabilities are from *Fischer and Tachiev* [2004] (A_1 and A_2), *Wiese et al.* [1996] for A_3 and *Slanger et al.* [2006] for A_4.

at 10 km from the nucleus as displayed in Figure 4. Regarding the oxygen state $O(^1S)$, radiative processes are effective above 20 km, and the maximum loss rate at 10 km above the nucleus reaches 2.62 s^{-1}.

Early results of the ROSINA/DFMS instrument have led to the unprecedented detection of N_2 in comets [*Rubin et al.*, 2015]. However, the relative abundance of this molecule is negligible (with a N_2/CO ratio of $(5.70 \pm 0.66) \times 10^{-3}$) for efficiently quenching the produced $O(^1D)$ and $O(^1S)$ since the rate coefficients for collisional processes with N_2 are similar to those with CO_2, as discussed by *Atkinson et al.* [2004]. Given the presence of O_2, two additional loss reactions have been considered, listed in Table 2. However, the impact of O_2 on the total loss rate, which is still dominated by the collisional quenching by water at low altitudes and by radiative decay otherwise, is negligible.

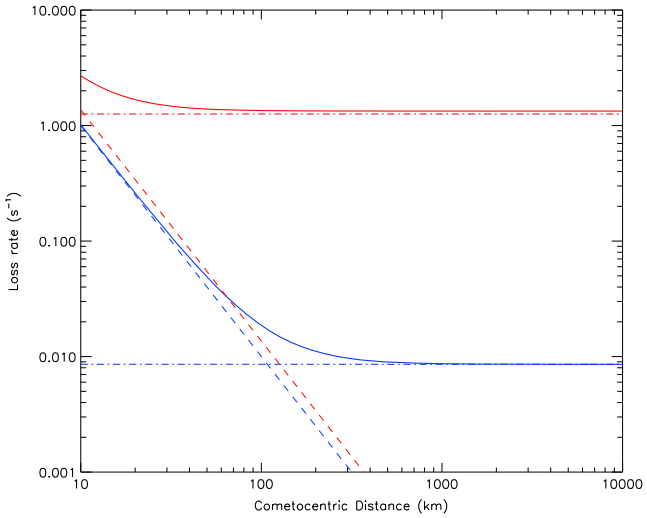

Figure 4. Total loss rates for $O(^1D)$ (thick blue) and $O(^1S)$ (thick red). The partial loss rates due to radiative decay (dash-dotted lines) and collision quenching by H_2O (dotted line) are also represented for $O(^1D)$ (blue) and $O(^1S)$ (red).

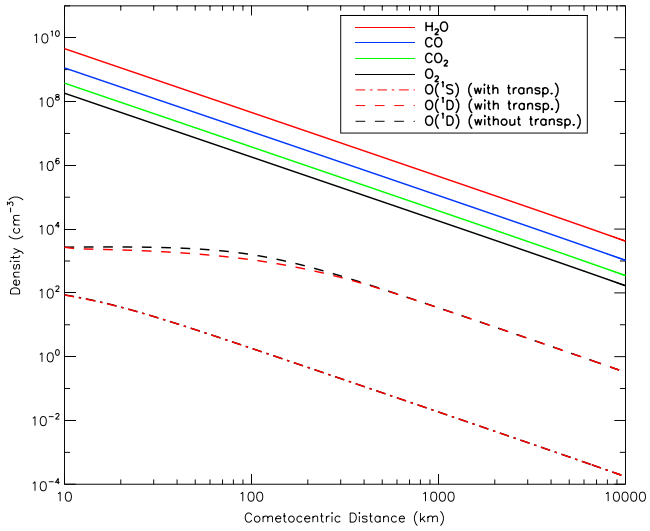

Figure 5. Number densities considered in the model based on the ROSINA/DFMS data and on Haser's formula, for water (red), CO (blue), O_2 (black), and CO_2 (green) using a water production rate of 4×10^{27} s^{-1} at 1.35 AU heliocentric distance. The computed number densities for $O(^1D)$ with (dash-dotted red line) and without transport (dashed black line) and for $O(^1S)$ (dash-dotted black line) are also displayed.

2.3. Red and Green Line Emissions

For evaluating the number densities of $O(^1D)$ and $O(^1S)$ within 67P, we solve the continuity equation using a constant radial outflow velocity, v, of 700 m s^{-1}, for steady state equations and spherical symmetry, such as

$$\frac{1}{r^2}\frac{d}{dr}(r^2 N_i v) = P_i - L_i \quad (3)$$

where N_i are the number densities for the excited atomic oxygen states, i.e., $O(^1D)$ and $O(^1S)$. P_i and L_i are the production and loss rates, respectively. The loss term, L_i, depends on the number densities, N_i. The equation has to be solved iteratively, starting from $z = 10$ km. The transport term will not impact the $O(^1S)$ density because its lifetime is very short (less than 1 s). This is not the case, however, for $O(^1D)$ with a lifetime of about 130 s, which represents a distance of 90 km for the considered velocity. The computed densities are displayed in Figure 5, along with the radial densities of water, carbon monoxide, carbon dioxide, and molecular oxygen used in our model. For the sake of comparison, the number density of $O(^1D)$ without transport is also represented.

The difference arising from the inclusion of transport is significant for altitudes lower than 400 km, with a maximum difference for the number density of $O(^1D)$ of 50% at 90–100 km. In the following, transport will therefore always be taken into account, unless specifically stated otherwise. The attenuation of the solar UV flux is not really pronounced, leading to a constant radial profile for $O(^1D)$ with a number density of about 2×10^3 cm^{-3} for altitudes below 100 km. The number density of $O(^1S)$ peaks at 10 km from the nucleus with a value close to 90 cm^{-3}.

Emission rate profiles for the red-doublet and green line can be deduced by multiplying the number densities with the Einstein transition probabilities indicated in Table 2 for reactions 4, 5, and 10. The green and red-doublet lines are forbidden transition and are therefore optically thin, making their attenuation by the cometary atmosphere negligible. The integrated emission intensity along a projected line-of-sight at various cometocentric distances, z, is an interesting parameter to be computed from our model for comparison to remote sensing observations. Considering the maximum extent of the coma to be less than 10^4 km, the computed emissions are estimated at 673 Rayleigh (R) and 493 R for $O(^1D)$ and $O(^1S)$, respectively, for $z = 10$ km. One Rayleigh (1 R) is defined as a column emission rate of 10^6 photons cm^{-2} s^{-1}. The computed emission intensities decrease at greater cometocentric distances: 508 R and 72 R for $O(^1D)$ and $O(^1S)$, respectively, for $z = 100$ km. We can also consider the green to red-doublet emission intensity ratio (G/R) as a function of the cometocentric distance. The G/R ratio is generally used for determining the CO_2 abundances in cometary atmospheres [*Decock et al.*, 2015]. We explore here the effect of transport on the G/R ratio, as displayed in Figure 6, considering an integration along the line of sight. With the number densities obtained in this work

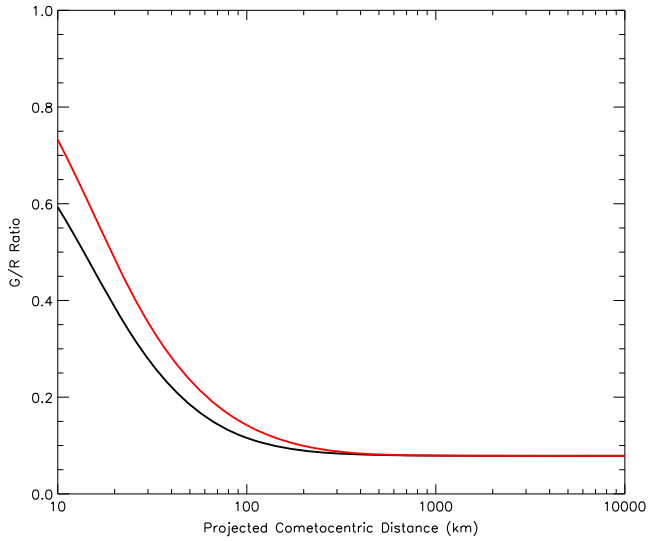

Figure 6. G/R ratio profile for 67P from 10 to 10^4 km for a line of sight crossing the projected cometocentric distance with (red) and without transport (black). The G/R ratio profile is calculated with a water production rate of 4×10^{27} s^{-1} for 25% CO, 8.3% CO_2, and 4% of O_2 abundances relative to water at 1.35 AU heliocentric distance.

for 67P, the G/R ratio peaks at 10 km with a value of 0.73 with transport and 0.59 without. By considering the transport, the G/R ratio increases along the line of sight below 400 km. The effect of transport will be important when the loss rate is dominated by collisional quenching. The gradient of the loss rate is large for altitudes lower than 400 km for O(^{1}D) (see Figure 4). At higher cometocentric distances, both ratios with and without transport are equivalent since the major loss reaction is the radiative decay process.

3. Discussion

Several parameters affect the number densities of O(^{1}D) and O(^{1}S), and therefore the G/R ratio. First, the distance to the Sun impacts directly the water production rate, Q, as well as the outgassing speed, v. These modifications affect the absorption of the solar UV flux at each altitude z, and therefore the reaction rate coefficients. The impact of transport depends on the outgassing speed. As discussed by *Bhardwaj and Raghuram* [2012], the production of O(^{1}S) through the photodissociation of H_2O depends on the chosen yield at the solar Lyman α line (set to be 0.5% in our model). The relative abundances of different elements also affect the G/R ratio. In the following, we still consider a distance to the Sun of 1.35 AU and we look for the impact of abundance variations for CO_2 and O_2. We also look for the choice of the partial cross sections for CO_2 and its implication on the G/R ratio. Finally, the G/R ratio will be characterized in a planetary space weather context by looking at the impact of solar activity on the photoproduction rates.

3.1. Impact of Cometary O_2

We first compare the computed G/R ratio obtained using the complete atmosphere of 67P including molecular oxygen from the previous sections to a molecular-oxygen-free atmosphere as displayed in Figure 7. While the G/R ratio peaks at 10 km with a value of 0.80 without O_2, it decreases down to 0.73 with O_2. Its presence thus induces a small difference in the G/R ratio profile. In order to assess whether this difference is significant, we consider a third atmospheric composition without oxygen, with the same CO abundance relative to water of 25% and a 6.3% CO_2 abundance relative to water. The computed G/R ratio profile is displayed in green in Figure 7. This 2% difference of CO_2 gives a similar profile as the one obtained with 8% of CO_2 and 4% of O_2. In the case of 67P with its atmospheric properties, not taking the presence of O_2 into account leads to an absolute underestimation of the CO_2 abundance relative to water of about 2%, which represents in fact a relative difference of 25%.

More generally, the increase of CO_2 alone leads to an enhancement of the G/R value, while it is the opposite for O_2 when using the reaction rate coefficients from Table 1. This is illustrated in Figure 8, where the G/R ratio is given for different configurations regarding the CO_2 (from 0% to 20%) and O_2 (0%, 4%, and 8%) abundances relative to water. For an amount of 16% of CO_2 at a distance of 10 km from the nucleus, the G/R ratio is about

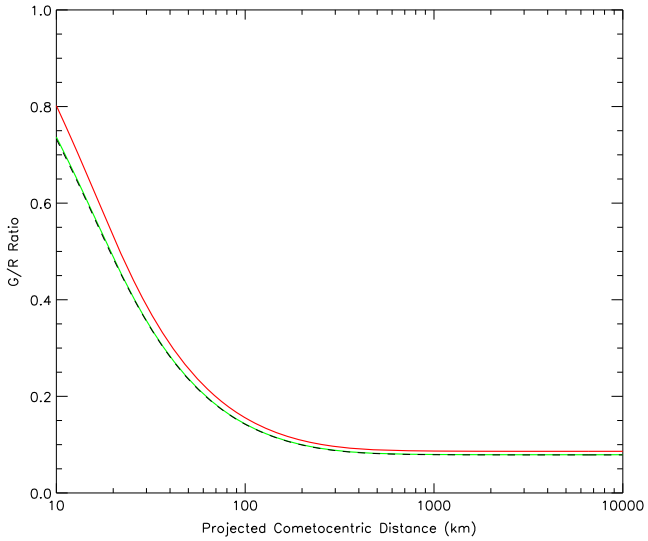

Figure 7. G/R ratio profile for 67P from 10 to 10^4 km for a line of sight crossing the projected cometocentric distance for several 67P atmospheric compositions: 8.3% CO_2 and 0% O_2 (red line), 8.3% CO_2 and 4% O_2 (dashed black line), and 6.3% CO_2 and 0% O_2 (green line). The G/R ratio profile is calculated with a water production rate of 4×10^{27} s^{-1} at 1.35 AU heliocentric distance.

1.02 with 0% of O_2. It decreases down to 0.94 for 4% of O_2 and down to 0.87 for 8% of O_2. At higher projected cometocentric distances, the presence of O_2 induces a smaller spread for the G/R ratio. At 50 km, the G/R ratio is of about 0.33, 0.30, and 0.28, still with 16% of CO_2 for an O_2 abundance of 0%, 4%, and 8%, respectively.

3.2. Impact of CO_2 Cross-Section Uncertainties

We consider from now on a complete 67P atmospheric composition including H_2O, CO_2 (8.3%), CO (25%), and O_2 (4%). The values found in the literature for the reaction rates of the production of oxygen states that $O(^1D)$ and $O(^1S)$ from photodissociation of CO_2 are actually quite diverse and, consequently, so is their ratio. This ratio is >1 in some studies [*Raghuram and Bhardwaj*, 2013], and <1 in others [*Bhardwaj and Raghuram*, 2012]. This difference comes from the chosen yield used for deducing the partial cross sections leading to the production of $O(^1D)$ and $O(^1S)$ from the total photoabsorption cross section of CO_2. To explore its impact on the G/R ratio, we consider here two extreme values, using two different cross-section sets for the photochemistry of carbon dioxide in our model. The first is the one used in the previous section. As a second cross-section data set, we consider the recommended values from the ATMOCIAD database. The $O(^1S)/O(^1D)$ ratio goes from 0.53 using the values provided in Table 1 to 6.98 using the cross sections from the ATMOCIAD database. The latter ratio is computed using photoreaction rates of 3.97×10^{-7} s^{-1} and 5.68×10^{-8} s^{-1} for $O(^1S)$ and $O(^1D)$, respectively, for a distance of 1.35 AU. Using such parameters, the computed emissions are estimated at 639 R and 571 R for $O(^1D)$ and $O(^1S)$, respectively, for $z = 10$ km. At this distance, the G/R ratio increases up to 0.89, compared to 0.73. Figure 9 displays the projected G/R ratio from 10 km to 10^4 km, using both cross-section data sets for a solar UV flux corresponding to an $F_{10.7}$ index of 104 (black lines). The lack of knowledge regarding the CO_2 cross sections thus leads to an important uncertainty on the computed G/R ratio and emphasizes the need for accurate CO_2 cross-section measurements.

3.3. Space Weather Context

Planetary space weather research has started with the exploration of planetary environments other than the Earth [*Lilensten et al.*, 2014]. It is today a growing research area of interest in the framework of future solar system missions such as JUICE [*Grasset et al.*, 2013] or BepiColombo [*Benkhoff et al.*, 2010]. In this context, we are looking at the impact of the solar UV flux variability, including the 11 year cycle and solar flares, on the G/R ratio. To do so, we consider here two additional solar UV values. The first one is a composite spectrum for a high but steady solar activity, with a $F_{10.7}$ solar proxy of 195 (red curve in Figure 2). The second one corresponds to the solar UV radiated during an X class solar flare (X17) measured by the TIMED/SEE spectrometer on 28 October 2003 green curve in Figure 2). The variability compared to quiet solar conditions can reach more than 1000% in the XUV spectral range between 0 and 20 nm, 100% in the EUV (20–120 nm), and 10–20% in the FUV (120–200 nm).

Figure 10 displays the different computed G/R ratios according to the different solar activity levels. We still consider both cross-section data sets regarding the production of $O(^1D)$ and $O(^1S)$ through the photodissociation of CO_2. The ratio generally increases for higher solar activity. With the ATMOCIAD database as inputs, the G/R ratio is of 1.55 for $z = 10$ km, while it is 1.08 using the PHIDRATES database for the X-17 solar flare. Observations of the red-doublet and green line emissions during a powerful solar flare could eventually help to constrain the reaction rates of the photodissociation of CO_2. Unfortunately, the solar flare must be "comet-effective," which is a rare event. Considering a less powerful X-1 solar flare from the 15 January 2005, the G/R ratio is still significantly impacted with values ranging from 1.21 to 0.091 using ATMOCIAD and PHIDRATES, respectively. The difference between G/R ratios using ATMOCIAD and PHIDRATES databases seems to increase when considering more powerful solar flare events. These results highlight the fact that more efforts are needed to better constrain the photodissociation cross sections of CO_2 leading to the production of $O(^1D)$ and $O(^1S)$, and solar flares could be a possible way for doing so.

There is also a noticeable impact of the 11 year cycle on the G/R ratio. The variability induced by such modulation is typically within 50–100% for the EUV, while it is less than 10% for the FUV. Between medium and high solar activity, the ratio increases from 0.73 to 0.86 (using PHIDRATES) and from 0.89 to 1.11 (using ATMOCIAD). However, this impact is actually hidden by the lack of knowledge on the cross sections. The solar irradiance is also impacted by a 27 day solar modulation from its rotation. However, the induced variability on the solar UV flux is not important enough to have a significant impact on the G/R ratio. Interestingly, this would mean that knowledge about the solar UV flux on a rotational time scale is not mandatory when considering the G/R ratio. It is, however, not the case for the number densities of $O(^1D)$ and $O(^1S)$, which are directly linked to the absolute solar UV values.

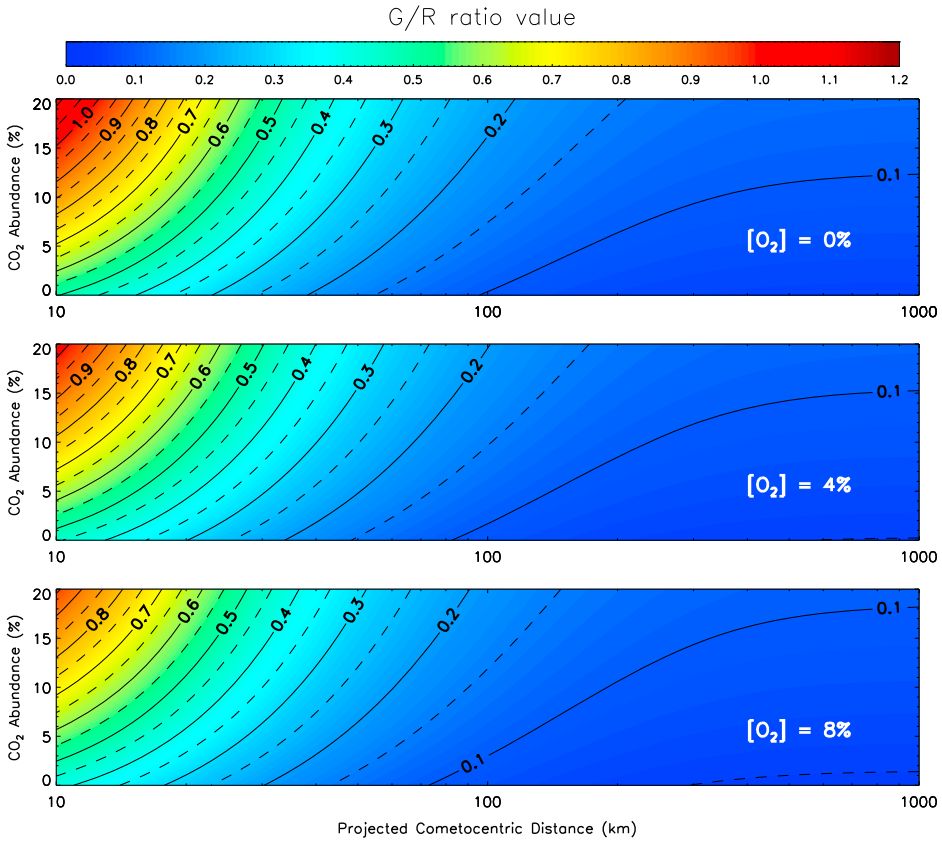

Figure 8. Modeled G/R ratio profile for 67P from 10 to 10^3 km for a line of sight crossing the projected cometocentric distance for several 67P atmospheric compositions regarding the CO_2 and O_2 abundances relative to water. The color code indicates the G/R ratio, which is calculated with a water production rate of 4×10^{27} s^{-1} at 1.35 AU heliocentric distance.

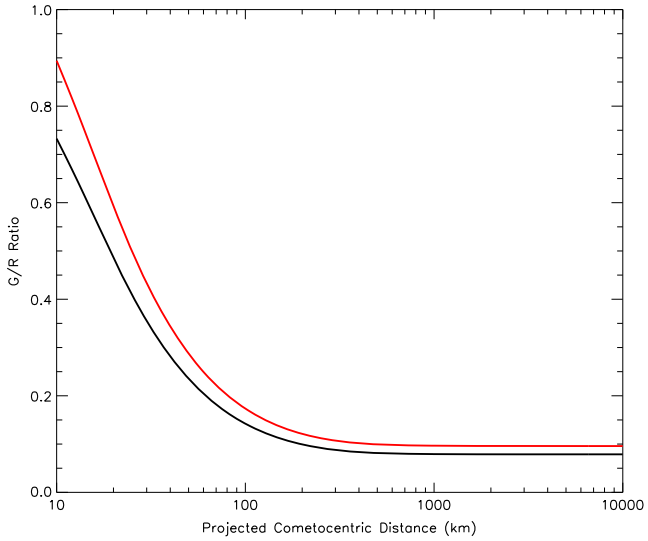

Figure 9. G/R ratio profile for 67P from 10 to 10^4 km for a line of sight crossing the projected cometocentric distance according to different cross section data sets for CO_2, using PHIDRATES (black) and ATMOCIAD (red). The G/R ratio profile is calculated with a water production rate of 4×10^{27} s^{-1} for 25% CO, 8.3% CO_2, and 4% of O_2 abundances relative to water at 1.35 AU heliocentric distance.

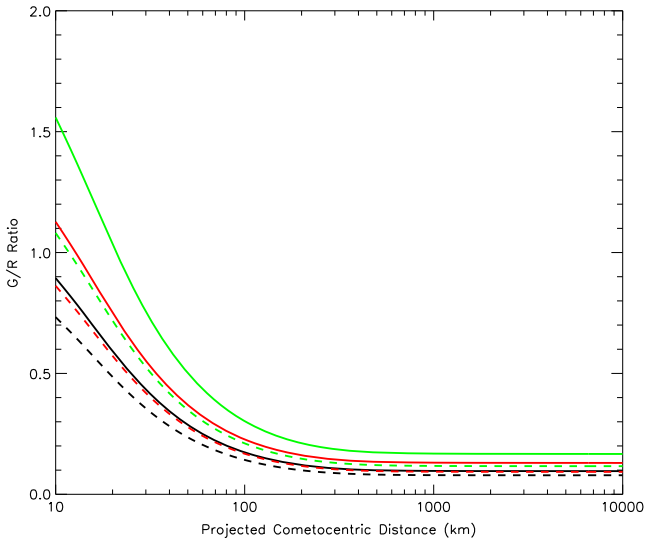

Figure 10. G/R ratio profile for 67P from 10 to 10^4 km for a line of sight crossing the projected cometocentric distance according to different levels of solar activity: for medium solar conditions with solar $F_{10.7}$ proxies of 104 (black lines) and 195 (red lines). The green lines correspond to the G/R ratio computed with the X17 solar flare spectrum as input. Dashed lines correspond to the computed G/R ratio using cross sections from PHIDRATES for CO_2, while solid lines use the ones from ATMOCIAD. The G/R ratio profile is calculated with a water production rate of 4×10^{27} s^{-1} for 25% CO, 8.3% CO_2, and 4% of O_2 abundances relative to water at 1.35 AU heliocentric distance.

4. Conclusions

We have presented in this paper a photochemistry-emission coupled model for the oxygen red-doublet and green lines for comet 67P/Churyumov-Gerasimenko. Using the ROSINA/DFMS data, an atmospheric composition based on water, CO_2, CO, and O_2 has been used. The latter species has never been taken into consideration in such modeling before. As outputs, we computed the G/R ratio along projected cometocentric distances; this G/R ratio has often been used for assessing the relative abundance of CO_2. However, the impact of O_2 is

strong enough to require a revision of such conclusions. The important results from our present study can be summarized as follows:

1. Not taking the transport of the produced $O(^1D)$ into account can lead to a significant underestimation of the G/R ratio for altitudes lower than 400 km, where most of the emission comes from. The transport can therefore not be neglected in such modeling.
2. CO_2 and O_2 have opposite effects on the G/R ratio. Not taking the presence of O_2 in cometary atmospheres into account would lead to an underestimation of its CO_2 abundance. The G/R ratio can therefore not be directly used for assessing the relative abundance of CO_2 within cometary atmospheres, without knowledge of the O_2 abundance.
3. CO_2 cross section uncertainties are high, and this requires more studies to better constrain the $O(^1D)$ and $O(^1S)$ production from the photodissociation of CO_2.
4. Within a space weather context, we have explored the effect of several solar conditions: a powerful flare has a significant impact on the G/R ratio, and can even be used as tool for constraining the CO_2 cross sections, assuming that the abundance of O_2 within the coma is known. Solar activity levels have to be characterized while measuring the G/R ratio.

The ROSINA/DFMS discovery of O_2 at a significant percentage might have been a surprise at first. The fact that O_2 had never been detected in a comet before seemed a major objection. In situ measurements at 1P/Halley with Giotto did not have sufficient mass resolution to really distinguish $^{16}O_2$ from ^{32}S and methanol (CH_3OH) [*Geiss et al.*, 1991], so its possible presence was simply overlooked. In remote sensing observations, no one has thought of including O_2 in emission models, so that these emissions were ascribed to CO_2, even when CO_2 itself was believed to be below the detection level (in the case of comet C/1996 B2 Hyakutake as modeled by *Bhardwaj and Raghuram* [2012]). Our findings that O_2 and CO_2 are in a sense interchangeable as far as the green and red line emissions are concerned are essential for understanding why measurements of the G/R ratio alone are insufficient to determine the presence or absence of either CO_2 or O_2—both are probably present but in an unknown proportion. Earlier assessments of CO_2 abundances in cometary atmospheres using the G/R ratio have to be revised in the light of the unambiguous O_2 detection by ROSINA/DFMS. This will be addressed in a forthcoming paper considering moderately and highly active comets using a 2-D photochemistry model for different CO_2 and O_2 abundances.

Acknowledgments
Work at BIRA-IASB was supported by the Fonds de la Recherche Scientifique grant PDR T.1073.14 comparative study of atmospheric erosion, by the Belgian Science Policy Office via PRODEX/ROSINAPEA4000107705 and an Additional Researchers grant (Ministerial Decree of 2014-12-19), and by the Interuniversitary Attraction Pole P7/15 "Planets: tracing the Transfer, Origin, Preservation and Evolution of their Reservoirs". Work at the ULB was supported by the Belgian Fund for Scientific Research - FNRS. Work at UoB was funded by the State of Bern, the Swiss National Science Foundation, and by the European Space Agency PRODEX Program. Work at Southwest Research Institute was supported by subcontract 1496541 from the Jet Propulsion Laboratory. Work at the University of Michigan was funded by NASA under contract JPL-1266313. G.G. was supported by NASA Astrobiology Institute grant NNX15AE05G and by the NASA HIDEE program. Rosetta is an ESA mission with contributions from its member states and NASA. The results from Rosetta and ROSINA would not be possible without the work of the many engineers, technicians, and scientists involved in the mission over the past 20 years, whose contributions are gratefully acknowledged. All Rosetta/ROSINA data are available on request until they are released to the PSA archive of ESA (www.rssd.esa.int/PSA) and to the PDS archive of NASA. The solar UV flux data were obtained from the LISIRD database (http://lasp.colorado.edu/lisird/ssi/). The cross-sections data used in this paper can be obtained from the PHIDRATES database (http://phidrates.space.swri.edu/), and from the ATMOCIAD database which is available from the authors upon request (Guillaume.P.Gronoff@nasa.gov). The authors would like to thank the anonymous reviewers for their insightful comments and suggestions that have contributed to improve this paper.

References

Altwegg, K., et al. (2015), 67P/Churyumov-Gerasimenko, a Jupiter family comet with a high D/H ratio, *Science*, *347*(27), 1261952, doi:10.1126/science.1261952.

Atkinson, R., D. L. Baulch, R. A. Cox, J. N. Crowley, R. F. Hampson, R. G. Hynes, M. E. Jenkin, M. J. Rossi, and J. Troe (2004), Evaluated kinetic and photochemical data for atmospheric chemistry: Volume I—Gas phase reactions of O_x, HO_x, NO_x and SO_x species, *Atmos. Chem. Phys.*, *4*(6), 1461–1738, doi:10.5194/acp-4-1461-2004.

Balsiger, H., et al. (2007), Rosina Rosetta orbiter spectrometer for ion and neutral analysis, *Space Sci. Rev.*, *128*, 745–801, doi:10.1007/s11214-006-8335-3.

Benkhoff, J., J. van Casteren, H. Hayakawa, M. Fujimoto, H. Laakso, M. Novara, P. Ferri, H. R. Middleton, and R. Ziethe (2010), BepiColombo-Comprehensive exploration of Mercury: Mission overview and science goals, *Planet. Space Sci.*, *58*, 2–20, doi:10.1016/j.pss.2009.09.020.

Bhardwaj, A., and S. Raghuram (2012), A coupled chemistry-emission model for atomic oxygen green and red-doublet emissions in the comet C/1996 B2 Hyakutake, *Astrophys. J.*, *748*, 13, doi:10.1088/0004-637X/748/1/13.

Bieler, A., et al. (2015), Abundant molecular oxygen in the coma of 67P/Churyumov-Gerasimenko, *Nature*, *526*(7575), 678–681.

Cochran, A. L. (2008), Atomic oxygen in the comae of comets, *Icarus*, *198*, 181–188, doi:10.1016/j.icarus.2008.06.007.

Decock, A., E. Jehin, D. Hutsemékers, and J. Manfroid (2013), Forbidden oxygen lines in comets at various heliocentric distances, *Astron. Astrophys.*, *555*, A34, doi:10.1051/0004-6361/201220414.

Decock, A., E. Jehin, P. Rousselot, D. Hutsemékers, J. Manfroid, S. Raghuram, A. Bhardwaj, and B. Hubert (2015), Forbidden oxygen lines at various nucleocentric distances in comets, *Astron. Astrophys.*, *573*, A1, doi:10.1051/0004-6361/201424403.

Evans, J. S., et al. (2015), Retrieval of CO_2 and N_2 in the Martian thermosphere using dayglow observations by IUVsS on MAVEN, *Geophys. Res. Lett.*, *42*, 9040–9049, doi:10.1002/2015GL065489.

Fischer, C. F., and G. Tachiev (2004), Breit-Pauli energy levels, lifetimes, and transition probabilities for the beryllium-like to neon-like sequences, *At. Data Nucl. Data Tables*, *87*(1), 1–184, doi:10.1016/j.adt.2004.02.001.

Geiss, J., K. Altwegg, E. Anders, H. Balsiger, A. Meier, E. G. Shelley, W.-H. Ip, H. Rosenbauer, and M. Neugebauer (1991), Interpretation of the ion mass spectra in the mass per charge range 25–35 amu/e obtained in the inner coma of Halley's comet by the HIS-sensor of the Giotto IMS experiment, *Astron. Astrophys.*, *247*, 226–234.

Grasset, O., et al. (2013), JUpiter ICy moons Explorer (JUICE): An ESA mission to orbit Ganymede and to characterise the Jupiter system, *Planet. Space Sci.*, *78*, 1–21, doi:10.1016/j.pss.2012.12.002.

Gronoff, G., C. S. Wedlund, C. J. Mertens, J. Lilensten, R. Lillis, and P. V. Johnson (2011), The AtMoCIAD database, paper presented at EPSC-DPS Joint Meeting, p. 1259, La Cité Internationale des Congrès Nantes Métropole, Nantes, France, 2–7 Oct.

Gronoff, G., C. Simon Wedlund, C. J. Mertens, and R. J. Lillis (2012a), Computing uncertainties in ionosphere-airglow models: I. Electron flux and species production uncertainties for Mars, *J. Geophys. Res.*, *117*, A04306, doi:10.1029/2011JA016930.

Gronoff, G., C. Simon Wedlund, C. J. Mertens, M. Barthélemy, R. J. Lillis, and O. Witasse (2012b), Computing uncertainties in ionosphere-airglow models: II. The Martian airglow, *J. Geophys. Res.*, *117*, A05309, doi:10.1029/2011JA017308.
Gronoff, G., A. Rahmati, C. S. Wedlund, C. J. Mertens, T. E. Cravens, and E. Kallio (2014), The precipitation of keV energetic oxygen ions at Mars and their effects during the comet Siding Spring approach, *Geophys. Res. Lett.*, *41*, 4844–4850, doi:10.1002/2014GL060902.
Haser, L. (1957), Distribution d'intensité dans la tête d'une comète, *Bull. Soc. R. Sci. Liege*, *43*, 740–750.
Hässig, M., et al. (2015), Time variability and heterogeneity in the coma of 67P/Churyumov-Gerasimenko, *Science*, *347*(1), aaa0276, doi:10.1126/science.aaa0276.
Huebner, W., and J. Mukherjee (2015), Photoionization and photodissociation rates in solar and blackbody radiation fields, *Planet. Space Sci.*, *106*, 11–45, doi:10.1016/j.pss.2014.11.022.
Huestis, D. L., T. G. Slanger, B. D. Sharpee, and J. L. Fox (2010), Chemical origins of the Mars ultraviolet dayglow, *Faraday Discuss.*, *147*, 307, doi:10.1039/c003456h.
Lee, L. C., T. G. Slanger, G. Black, and R. L. Sharpless (1977), Quantum yields for the production of $O(^1D)$ from photodissociation of O_2 at 1160–1770 Å, *J. Chem. Phys.*, *67*, 5602–5606.
Le Roy, L., et al. (2015), The inventory of the volatiles on comet 67P/Churyumov-Gerasimenko from Rosetta/Rosina, *Astron. Astrophys.*, *583*, A1, doi:10.1051/0004-6361/201526450.
Lilensten, J., A. J. Coates, V. Dehant, T. Dudok de Wit, R. B. Horne, F. Leblanc, J. Luhmann, E. Woodfield, and M. Barthélemy (2014), What characterizes planetary space weather?, *Astron. Astrophys. Rev.*, *22*, 79, doi:10.1007/s00159-014-0079-6.
McClintock, W. E., M. Snow, and T. N. Woods (2005), Solar-stellar irradiance comparison experiment II (SOLSTICE II): Pre-launch and on-orbit calibrations, *Sol. Phys.*, *230*, 259–294, doi:10.1007/s11207-005-1585-5.
McKay, A., A. Cochran, M. DiSanti, G. Villanueva, N. Dello Russo, R. Vervack, J. Morgenthaler, W. Harris, and N. Chanover (2015), Evolution of H_2O, CO, and $\{CO_2\}$ production in comet c/2009 {P1} garradd during the 2011;-2012 apparition, *Icarus*, *250*, 504–515, doi:10.1016/j.icarus.2014.12.023.
McKay, A. J., N. J. Chanover, J. P. Morgenthaler, A. L. Cochran, W. M. Harris, and N. D. Russo (2012), Forbidden oxygen lines in Comets C/2006 W3 Christensen and C/2007 Q3 Siding Spring at large heliocentric distance: Implications for the sublimation of volatile ices, *Icarus*, *220*, 277–285, doi:10.1016/j.icarus.2012.04.030.
McKay, A. J., N. J. Chanover, J. P. Morgenthaler, A. L. Cochran, W. M. Harris, and N. D. Russo (2013), Observations of the forbidden oxygen lines in DIXI target Comet 103P/Hartley, *Icarus*, *222*, 684–690, doi:10.1016/j.icarus.2012.06.020.
Morgenthaler, J. P., W. M. Harris, and M. R. Combi (2007), Large aperture [OI] 6300 Å observations of comet Hyakutake: Implications for the photochemistry of OH and [OI] production in comet Hale-Bopp, *The Astrophys. J.*, *657*(2), 1162–1171.
Raghuram, S., and A. Bhardwaj (2013), Model for atomic oxygen visible line emissions in Comet C/1995 O1 Hale-Bopp, *Icarus*, *223*, 91–104, doi:10.1016/j.icarus.2012.11.032.
Raghuram, S., and A. Bhardwaj (2014), Photochemistry of atomic oxygen green and red-doublet emissions in comets at larger heliocentric distances, *Astron. Astrophys.*, *566*, A134, doi:10.1051/0004-6361/201321921.
Rottman, G. (2005), The SORCE mission, *Sol. Phys.*, *230*, 7–25, doi:10.1007/s11207-005-8112-6.
Rubin, M., et al. (2015), Molecular nitrogen in comet 67P/Churyumov-Gerasimenko indicates a low formation temperature, *Science*, *348*, 232–235, doi:10.1126/science.aaa6100.
Slanger, T. G., P. C. Cosby, B. D. Sharpee, K. R. Minschwaner, and D. E. Siskind (2006), $O(^1S \rightarrow {}^1D, {}^3P)$ branching ratio as measured in the terrestrial nightglow, *J. Geophys. Res.*, *111*, A12318, doi:10.1029/2006JA011972.
Wiese, W. L., J. R. Fuhr, and T. M. Deters (1996), Atomic transition probabilities of carbon, nitrogen, and oxygen: A critical data compilation, in *Journal of Physical and Chemical Reference Data Monograph*, p. 522, Am. Chem. Soc. and Am. Inst. Phys., Woodbury, N. Y.
Woods, T. N., F. G. Eparvier, S. M. Bailey, P. C. Chamberlin, J. Lean, G. J. Rottman, S. C. Solomon, W. K. Tobiska, and D. L. Woodraska (2005), Solar EUV Experiment (SEE): Mission overview and first results, *J. Geophys. Res.*, *110*, A01312, doi:10.1029/2004JA010765.
Woods, T. N., et al. (2008), XUV Photometer System (XPS): Improved solar irradiance algorithm using CHIANTI spectral models, *Sol. Phys.*, *250*, 235–267, doi:10.1007/s11207-008-9196-6.

Erratum

In the originally published version of this article, a measurement of tolerance in the abstract and in section 2 was missing a percentage sign (%). In addition, Figures 6, 8, 9, 10 had correct legends but the incorrect images appeared with them. These errors have since been corrected, and this version may be considered the authoritative version of record.

The originally published image for Figure 6 now correctly appears as Figure 10.

The originally published image for Figure 8 now correctly appears as Figure 9.

The originally published image for Figure 9 now correctly appears as Figure 6.

The originally published image for Figure 10 now correctly appears as Figure 8.